Journal of Alloys and Compounds 504S (2010) S69–S73

Contents lists available at ScienceDirect

Journal of Alloys and Compounds

journal homepage: www.elsevier.com/locate/jallcom

The study of loading rate effect of a Cu-based bulk metallic glass during nanoindentation

K.W. Chen[a], S.R. Jian[b], P.J. Wei[c], J.S.C. Jang[d], J.F. Lin[a,e,*]

[a] Department of Mechanical Engineering, National Cheng Kung University, Tainan 701, Taiwan
[b] Department of Materials Science and Engineering, I-Shou University, Kaohsiung 840, Taiwan
[c] Institute of Nanotechnology and Microsystems Engineering, National Cheng Kung University, Tainan 701, Taiwan
[d] Department of Mechanical Engineering, Institute of Materials Science & Engineering, National Central University, Chung-Li 320, Taiwan
[e] Center for Micro/Nano Science and Technology, National Cheng Kung University, Tainan 701, Taiwan

ARTICLE INFO

Article history:
Received 3 July 2009
Received in revised form 22 March 2010
Accepted 29 March 2010
Available online 3 April 2010

Keywords:
Metals
Amorphous materials
Scanning and transmission electron microscopy

ABSTRACT

In this study, the nanoindentation behavior of a Cu–Zr–Al–Ag bulk metallic glass was investigated at various loading rates. It is found that the load–displacement curve of indentation exhibits a significant serration of displacement jumps (pop-ins). The experiment data show that the depths of the pop-in site are a geometric series. The size of pop-ins increases with indentation depth but decreases with loading rate; a larger applied loading rate leads to smaller pop-ins during the indentation process. However, the experimental results indicate that the loading rate has no influence on the depth ratio of pop-in sites. FIB observation and TEM diffraction patterns show that the microstructure of the BMG material remained amorphous irrespective of the presence shear bands.

1. Introduction

Bulk metallic glasses (BMGs) have received a great deal of attention due to their interesting properties, such as amorphous microstructure, ultra-high strength, and excellent corrosion resistance [1–3]. The mechanical properties of amorphous alloys are unlike those of crystalline ones. BMGs are relatively brittle compared to their crystalline counterparts at room temperature. This lack of plasticity currently limits the structural applications of BMGs [4]. BMGs tend to form semicircular shear bands at room temperature when high pressure induced localized deformation occurs [5,6]. Because of strain softening, the formation of shear bands reduces the strength of BMGs, which leads to brittle fractures along the shear planes [7]. Thus, avoiding large shear bands is crucial for structural and engineering applications of BMGs.

Indentation surveys are widely applied to characterize the mechanical properties of BMGs. It was found that the hardness of the shear band zone beneath the indentation cavity is smaller than that of the area without deformation because of deformation-induced softening [8]. Some researchers reported that the load–displacement curve (p–h curve) of BMGs during the indentation process exhibits displacement bursts, known as "pop-ins" or "serrations" [9–17]. They also observed that the pop-in size varies with indentation depth and indentation loading rate. Nieh suggested that the pop-ins are associated with the emission of shear bands [16]. Schuh generated a deformation mechanism map for BMGs [17]. However, no mathematical relationship between shear bands and pop-ins has been proposed.

In order to estimate the mathematical relationship between shear bands and pop-ins for BMGs, we developed an analytical model to predict the radii in semicircular shear bands, known as primary shear band circles, and found that the relationship of these radii is a geometric series with a common ratio. The proposed model indicates that the relationship of pop-in sites is also a geometric series, which has the same common ratio as that of the radius geometric series. This result directly proves that the formation of pop-ins is due to the emission of shear bands. In addition, most previous studies reported that the pop-in size varies with loading rate during indentation process. Thus, the loading rate effect is also discussed for the proposed analytical model.

2. Model derivation for shear band circles

Shear band formations in indentations are known to be the dominant deformation mechanism at room temperature. Fig. 1(a) shows the free body diagram of a shear band annulus. The pressure, σ_r, acting at outer surface of the annulus can be integrated as the upward

* Corresponding author at: Department of Mechanical Engineering, National Cheng Kung University, No. 1, University Road, Tainan 701, Taiwan.
Tel.: +886 6 2757575x62155.
E-mail address: jflin@mail.ncku.edu.tw (J.F. Lin).

0925-8388/$ – see front matter © 2010 Elsevier B.V. All rights reserved.
doi:10.1016/j.jallcom.2010.03.207

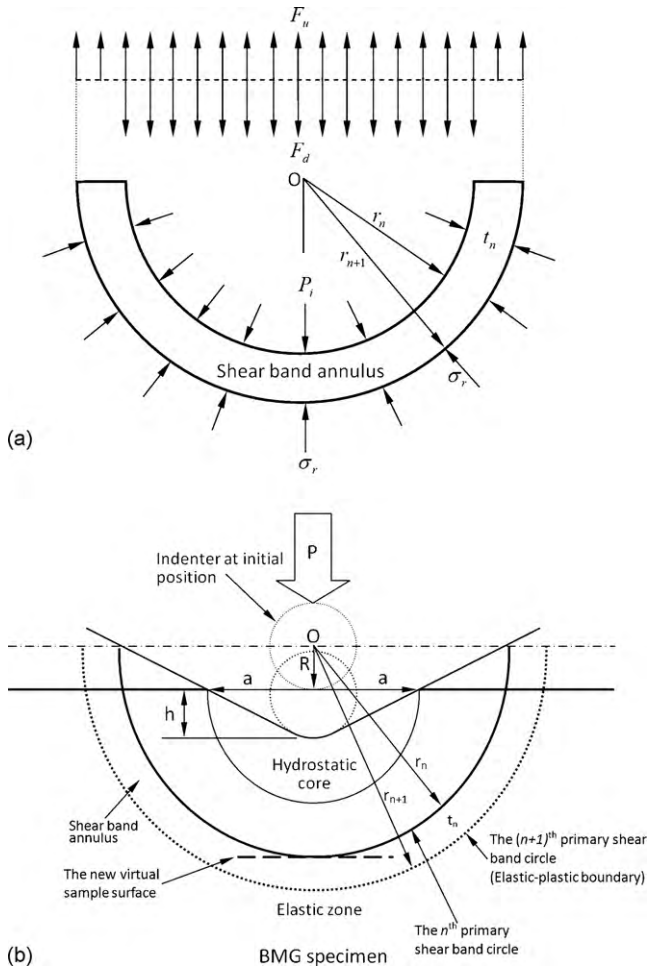

Fig. 1. Schematic of the indentation of a BMG surface.

force F_u in the vertical direction. The pressure acting at inner surface of the annulus can be integrated as the downward force F_d in vertical direction. Fig. 1(b) shows a schematic diagram of an indentation on a BMG specimen. Many semicircular shear bands are created beneath the indenter when an indentation load P is applied. In Fig. 1(b), the radius of the nth shear band circle is r_n, and the annulus width between the nth and $(n+1)$th shear band circles is t_n. The tips of Vickers and Berkovich indenters can be roughly treated as spherical indenters with a radius of curvature. Once the semicircular shear band forms, this shear band circle can be treated as a new virtual round indenter. Therefore, both Vickers and Berkovich indentation can be treated as spherical indentation in whole indentation process. The radius of the real contact area is a, and the real indentation depth is h. The whole indentation process is performed at room temperature and the shear band circle is formed once the plastic deformation occurs. For the annulus between the nth and $(n+1)$th shear band circles, the force balance in the vertical direction satisfies:

$$\sum F_v = 0 \tag{1}$$

In Fig. 1(a), the downward force can be calculated as $F_d = P_i \pi r_n^2$. Similarly, the upward force can be determined as $F_u = \sigma_r \pi r_{n+1}^2$, where $r_{n+1} = r_n + t_n$. Then, Eq. (1) can be rewritten as follows:

$$P_i \pi r_n^2 = \sigma_r \pi (r_n + t_n)^2 \tag{2}$$

Therefore,

$$\frac{P_i}{\sigma_r} = \left(\frac{r_n + t_n}{r_n}\right)^2 \tag{3}$$

According to the cavity model in contact mechanics, the stress acting at the elastic-plastic boundary can be determined as $\sigma_r = 2Y/3$, where Y denotes the yield strength of the material. Define P_m as the mean pressure acting on the contact area in Fig. 1(b). Then, the mean pressure P_m is equal to the hardness (H) of the specimen when the specimen starts to yield. In the present model, the nth shear band circle is treated as the virtual round indenter with the tip radius of r_n. This viewpoint indicates that $P_i = P_m = H'$, where H' denotes the hardness obtained using the virtual indenter. Since the yield strength and the hardness of a material are constants, the term $(r_n + t_n)/r_n$ in the right-hand side of Eq. (3) is also ensured to be a positive constant value (c). Then, the solutions of t_n can be expressed as follows:

$$t_n = (C-1)\, r_n \tag{4}$$

The radius of the $(n+1)$th shear band circle is thus written as follows:

$$r_{n+1} = r_n + t_n = r_n + (C-1)\, r_n = C r_n \tag{5}$$

Therefore,

$$\frac{r_{n+1}}{r_n} = C\ ,\ \ n = 1, 2, 3, \ldots \tag{6}$$

Using the induction method, the nth shear band circle has a radius (r_n) expressed as a function of the radius of the first shear band circle (r_1) as follows:

$$r_n = C^{n-1} r_1 \tag{7}$$

Using the contact mechanics shown in the study of Bei et al. [18], the first shear band circle initiates at the interface between the elastic zone and the plastic zone, which is located at the position $z \cong 0.5a$. Therefore, the radius of the first shear band circle is $r_1 \cong 0.5a + R$. Define the radius of the indenter's round tip as R; then, $a = \sqrt{Rh}$ [19]. After a shear band circle forms, the largest shear band circle is viewed as a virtual spherical indenter. This new virtual spherical indenter continuously indents the new virtual surface (as shown in Fig. 1). The derivation below is used to obtain the ratio of the indentation depths corresponding to any two adjacent pop-ins as a function of the C parameter. r_1 can be expressed as follows:

$$r_1 = 0.5\sqrt{Rh_1} + R \tag{8}$$

where h_1 is the indentation depth corresponding to the radius of the shear band circle r_1. Then, r_n ($n = 1, 2, 3, \ldots$) can be expressed as follows:

$$r_2 = 0.5\sqrt{r_1 h_2} + r_1 \tag{9.a}$$

$$r_3 = 0.5\sqrt{r_2 h_3} + r_2 \tag{9.b}$$

$$\vdots$$

$$r_{n+1} = 0.5\sqrt{r_n h_{n+1}} + r_n \tag{9.n}$$

The above expressions are obtained with the assumption that the annulus between any two adjacent shear band circles (with radii r_{n+1} and r_n) is subjected to an indentation load applied by an indenter with a radius of r_n. Actually, this radius is virtual. The second term on the right-hand side of Eq. (9.a) to Eq. (9.n) represents the indenter tip's movement from the origin O to a point beneath point O with a distance t_n ($n = 1, 2, 3, \ldots$). Since $r_{n+1} = Cr_n$ ($n = 1, 2, 3, \ldots$), the left-hand side of Eq. (9) becomes:

$$Cr_n = 0.5\sqrt{r_n h_{n+1}} + r_n \quad (n = 1, 2, 3, \ldots) \tag{10}$$

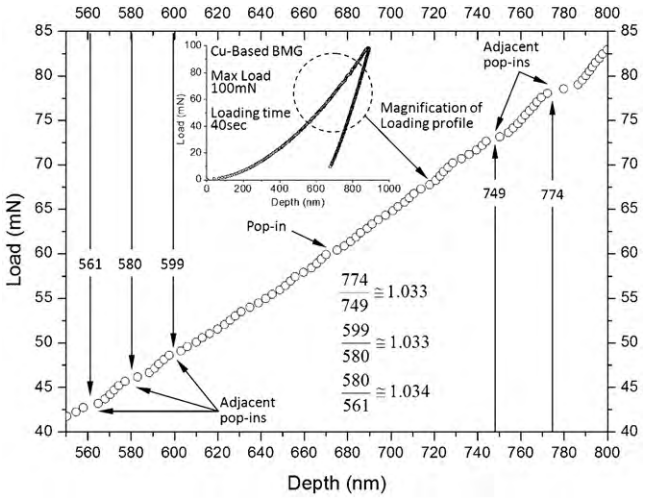

Fig. 2. Nanoindentation p–h curve of $Cu_{42}Zr_{42}Al_8Ag_8$ BMG.

Eq. (10) can be rewritten as follows:

$$4r_n(C-1)^2 = h_{n+1} \quad (n = 1, 2, 3, \ldots) \tag{11}$$

Therefore,

$$\frac{h_{n+2}}{h_{n+1}} = \frac{4r_{n+1}(C-1)^2}{4r_n(C-1)^2} = \frac{r_{n+1}}{r_n} = C \tag{12}$$

The indentation depths corresponding to two adjacent pop-ins are thus available for determining the C value shown in Eq. (12). Then, the relationship $h_{n+2}/h_{n+1} = h_{n+1}/h_n = C$, shown in Eq. (12), can be used to determine all indentation depths corresponding to all pop-ins shown in the loading process of the p–h curve. The validity of the indentation depth of pop-ins predicted by the present model can be checked from the pop-in positions shown in the experimental p–h curve.

3. Experimental details

Cu-based BMG ($Cu_{42}Zr_{42}Al_8Ag_8$) was used in the present study. MTS indentation tests (MTS Nano Indenter XP, USA) were performed under basic mode with a maximum load of 100 mN and various loading times (2.5, 5, 10, 20, 40 s). The radius of the indenter tip was about 150 nm. The thermal drift was controlled to be below 0.15 nm/s. The bonded interface technique [5,6,8,15] for Vickers indentation was used in the present study. A maximum load of 500 gf (approximately 4900 mN) and a loading time of 15 s were applied in the Vickers indentation tests. The TEM specimens were prepared using a dual beam focused ion beam (DB-FIB) system. In order to protect the original microstructure from ion bombardment damage, a 1.5-μm thick platinum layer was deposited as the protective layer before the TEM sampling procedure was performed. Then, the microstructures of the Cu-based BMG beneath the indentation cavity were examined using FEI Tecnai G^2 20 S-Twin TEM.

4. Results and discussion

Eq. (12) indicates that if pop-ins in the p–h curve are due to the formation of shear bands during the indentation process, the depth ratio of pop-ins and the radius ratio of shear band circles have the same factor, C. Fig. 2 shows a magnification of the Cu-based BMG nanoindentation p–h curve in the depth range of 550–800 nm. There are six noticeable pop-ins in the p–h curve, five of which are adjacent. The depth ratios of two adjacent pop-ins in Fig. 2 are 1.033, 1.033, and 1.034, which are almost equal. This result confirms the equality $h_{n+2}/h_{n+1} = C$ in Eq. (12) and shows that the value $C = 1.033$. Because the shear bands pattern created by MTS nanoindentation was too small to be visible, we performed Vickers microindentation to produce a better pattern of shear bands.

In Fig. 3, the shear band circles formed nearby the tip region of the indentation cavity are seen to be quite crowded together and not so smooth in curved profiles. Therefore, it is difficult to measure the radii of these shear band circles precisely. We are forced to mark the values only for the shear bands which are distinguishable clearly in radius. The radius ratios evaluated at these successive shear band circles are in a range of 1.033–1.039. The mean value (1.035) of these ratios is quite close to these values. This result confirms the equality $r_{n+1}/r_n = C$ in Eq. (12) and is approximately the value exhibited by the depth ratio of pop-ins. That is, the experimental results of micro-/nano-indentations confirm the validity of the proposed analytical model, and show that the pop-ins in the p–h curve are due to the formation of shear bands.

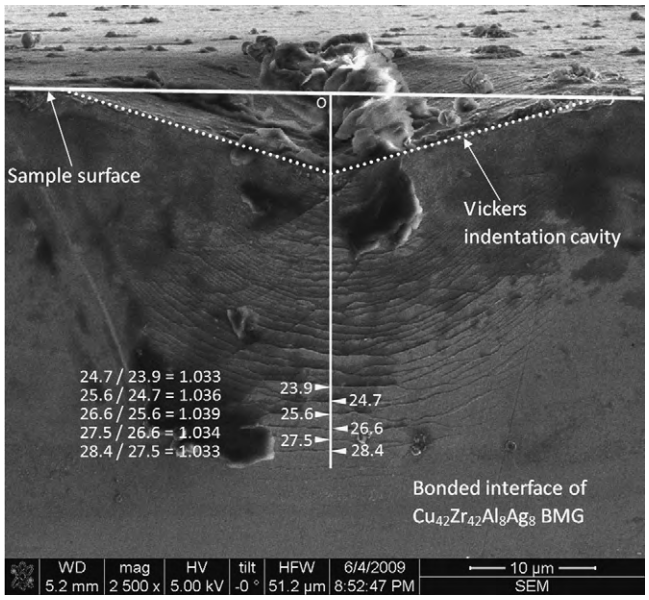

Fig. 3. FIB image of shear bands pattern from Vickers indentation.

Fig. 4 shows the p–h data recorded during nanoindentation to a maximum load of 100 mN for a variety of constant loading times (from 2.5 to 40 s). Each data point was shifted 200 nm for clarity. Because the sampling frequency of the instrument was fixed at 5 Hz under basic mode, a larger loading time produced more data. In Fig. 4, the serrations are more noticeable at a lower loading rate. Fig. 5 shows the normalized serration size, h_{jump}/h, as a function of the indentation loading rate. The normalized pop-in size approximately linearly decreases with applied loading rate in indentation process. Yang and Nieh [20] have also reported that the p–h curves

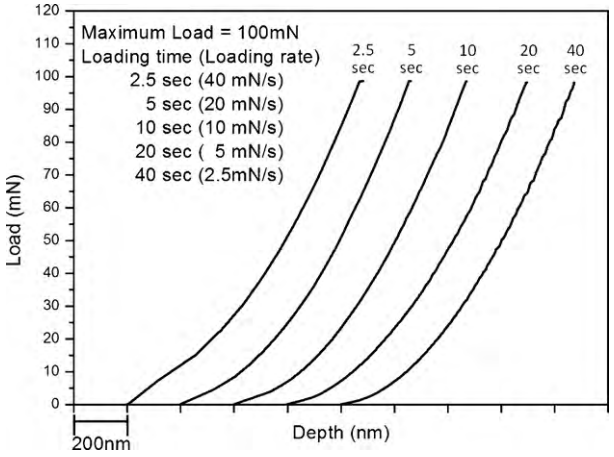

Fig. 4. p–h data recorded during nanoindentation to a maximum load of 100 mN for various loading times (from 2.5 to 40 s). Each data point was shifted by 200 nm.

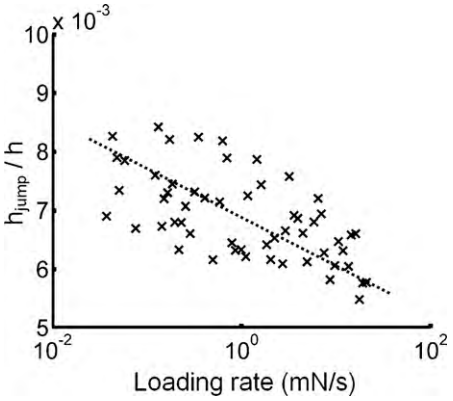

Fig. 5. Normalized serration size as a function of indentation loading rate.

of pop-ins become smooth with increasing the loading rate. This result shows that the serrations (or pop-ins) will disappear if the loading rate is high enough. Some researchers have reported similar experimental results [11,12].

Fig. 6 shows the serration size (or pop-in size) as a function of loading depth. In this figure, the pop-in size scaling is approximately linear. In the present study, the slope of h_{jump}/h is 0.0076 within a depth range of 0–1000 nm. The proposed model shows that pop-ins are due to the formation of shear bands, so it is reasonable to expect that larger pop-ins correspond to greater shear displacements within the shear bands. This result is consistent with that reported by Schuh and Nieh [16].

Fig. 7 shows the penetration rate (or penetration velocity) of the indenter as a function of indentation depth. Each peak in the curves represents a displacement burst (or pop-in). These peaks can be used to clearly identify pop-in sites. Fig. 7(a) and (b) shows indentation loading times of 20 s (5 mN/s in loading rate) and 40 s (2.5 mN/s in loading rate), respectively. The depth ratios are also calculated and shown in this figure. Because the indentation experiments were carried out in a mode of constant loading rate, the rates of penetration depth occurring in the small depth region were much higher than that in the large depth region. However, the sampling rate of the MTS XP mode is 5 Hz only. The inconsistency between them causes the difficult to achieve accurate position successive pop-ins if the loading rate is too high. This is the reason why no value is given for the peaks in Fig. 7(a) present in the small depth region. In Fig. 7(a), only five depth ratios of the pop-ins at large

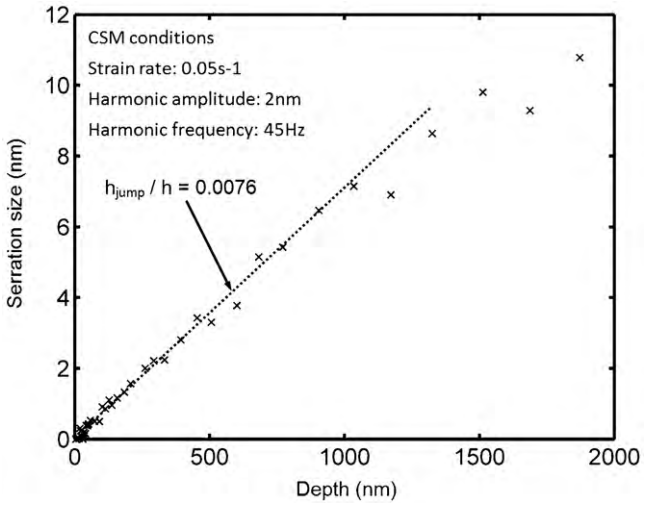

Fig. 6. Serration size as a function of loading depth.

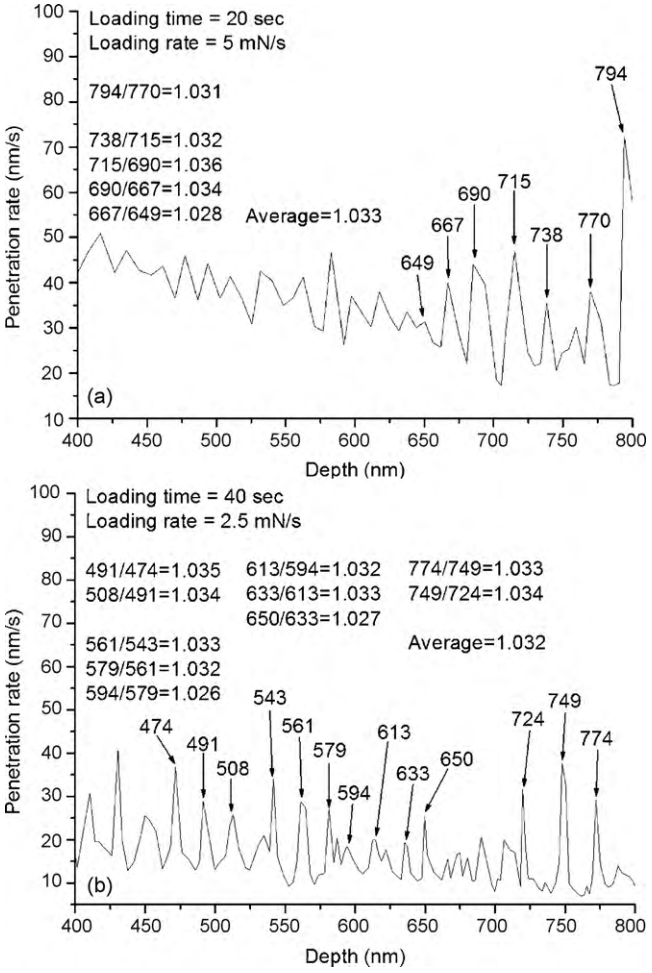

Fig. 7. Penetration rate of the indenter as a function of indentation depth for (a) loading time of 20 s (5 mN/s) and (b) loading time of 40 s (2.5 mN/s).

depth are calculated to be in a range of 1.028–1.036; an average value of 1.033 was obtained. In Fig. 7(b), ten depth ratios of successive pop-ins are in a range of 1.026–1.035, for an average value of 1.032. The difference between these two average values is insignificant. This result indicates that despite the pop-in size decreasing with loading rate, the depth ratio of pop-ins is independent of the loading rate. Thus, this result also confirms that the constant C represents the material property. However, the pop-in site will be difficult to identify if the applied loading rate is too large. We suggest using a smaller loading rate to obtain larger data density and more accurate pop-in sites.

Fig. 8 shows the TEM bright field view of $Cu_{42}Zr_{42}Al_8Ag_8$ after the nanoindentation test. A residual indentation cavity can be clearly observed. However, the shear bands pattern created by nanoindentation is too small to be visible. The microstructure of Cu-based BMG beneath the cavity is well protected from ion bombardment damage. However, the diffraction pattern near the tip of indentation cavity (denoted by "A") indicates that the microstructure is still amorphous. In location B, far away from the tip of cavity, the microstructure remains amorphous after the indentation test. This result shows that $Cu_{42}Zr_{42}Al_8Ag_8$ BMG has neither a crystallization nor phase change in the shear band zone. The generation of shear band circles is simply related to the yielding behavior of the present material, rather than the crystallization that occurs in the microstructure. Similar behavior was reported in the study of Puthucode et al. [14] for a Zr-based BMG.

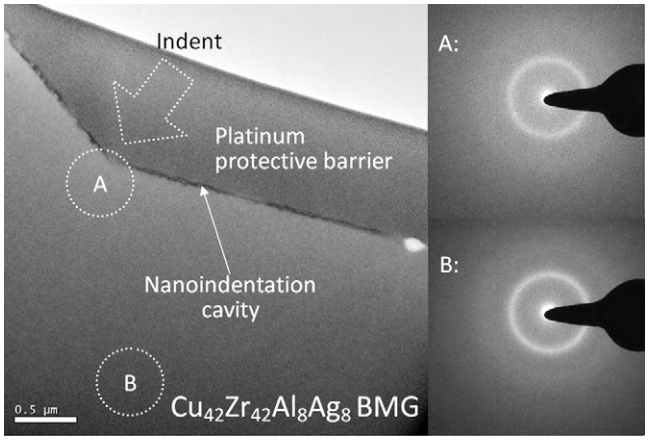

Fig. 8. TEM bright field view of $Cu_{42}Zr_{42}Al_8Ag_8$ BMG after MTS nanoindentation test. The selected area diffraction patterns (SADP) shown in the figure are corresponding to the regions A and B beneath the indentation cavity, respectively.

5. Conclusion

1. The proposed analytical model shows that the radii of shear band circles and the depths of pop-ins sites are geometric series with a common ratio of *C*. This result indicates that pop-ins in the loading *p–h* curve are a result of shear band deformation.
2. The radius ratio of any two adjacent shear band circles is a constant value, which can be obtained using any two adjacent pop-ins in the loading stage of nanoindentation. Experimental results show that the pop-in size increases with indentation depth and decreases with loading rate. However, the indentation loading rate does not affect the depth ratio of pop-ins.
3. TEM diffraction patterns show that the microstructure of the Cu-based BMG remained amorphous regardless of shear band formation. The generation of shear band circles is related to cracking behavior rather than crystallization.

Acknowledgements

This work was partially supported by the National Science Council of Taiwan, under Grant No.: NSC97-2112-M-214-002-MY2.

References

[1] A. Inoue, Acta Mater. 48 (2000) 279–306.
[2] A. Inoue, B.L. Shen, H. Koshiba, H. Kato, A.R. Yavari, Acta Mater. 52 (2004) 1631–1637.
[3] J.R. Scully, A. Gebert, J.H. Payer, J. Mater. Res. 22 (2007) 302–313.
[4] J. Eckert, J. Das, S. Pauly, C. Duhamel, J. Mater. Res. 22 (2007) 285–301.
[5] S. Jana, R. Bhowmick, Y. Kawamura, K. Chattopadhyay, U. Ramamurty, Intermetallics 12 (2004) 1097–1102.
[6] S. Jana, U. Ramamurty, K. Chattopadhyay, Y. Kawamura, Mater. Sci. Eng. A 375–377 (2004) 1191–1195.
[7] H. Bei, S. Xie, E.P. George, Phys. Rev. Lett. 96 (2006) 105503, 4 pp.
[8] B.G. Yoo, J. Jang, J. Phys. D: Appl. Phys. 41 (2008) 074017, 7 pp.
[9] L. Liu, K.C. Chan, Mater. Lett. 59 (2005) 3090–3094.
[10] Z.L. Chen, X.D. Mei, Z.T. Hua, W.B. Chen, L.W. Huo, W.Y. Ren, Chin. Sci. Bull. 51 (2006) 1639–1643.
[11] S.X. Song, J.S.C. Jang, T.G. Nieh, Intermetallics 16 (2008) 676–681.
[12] T. Burgess, K.J. Laws, M. Ferry, Acta Mater. 56 (2008) 4829–4835.
[13] B.G. Yoo, K.W. Lee, J. Jang, J. Alloy Compd. (2008), doi:10.1016/j.jallcom.2008.07.163.
[14] A. Puthucode, R. Banerjee, S. Vadlakonda, R. Mirshams, M.J. Kaufman, Metal. Mater. Trans. A 39 (2008) 1552–1559.
[15] H. Xie, Y. Li, D. Yang, P. Hodgson, C. Wen, J. Alloy. Compd. 475 (2009) 501–505.
[16] C.A. Schuh, T.G. Nieh, Acta Mater. 51 (2003) 87–99.
[17] C.A. Schuh, T.G. Nieh, J. Mater. Res. 19 (2004) 46–57.
[18] H. Bei, Z.P. Lu, E.P. George, Phys. Rev. Lett. 93 (2004) 125504, 4 pp.
[19] A.C. Fischer-Cripps, Nanoindentation, Springer, NY, 2004, pp. 8–9.
[20] B. Yang, T.G. Nieh, Acta Mater. 55 (2007), 295–200.